Journal of Applied Electrochemistry **33**: 1191–1198, 2003.

Methanol oxidation at $Pt/MoO_x/MoSe_2$ thin film electrodes prepared with exfoliated $MoSe_2$

H. BOLIVAR, S. IZQUIERDO, R. TREMONT and C.R. CABRERA*
*Department of Chemistry, University of Puerto Rico, Río Piedras Campus, San Juan, Puerto Rico 00931-3346, USA (*author for correspondence, e-mail: ccabrera@goliath.cnnet.clu.edu)*

Received 17 October 2002; accepted in revised form 26 July 2003

Key words: exfoliation, methanol oxidation, Mo, $MoSe_2$, Pt

Abstract

This paper presents results on the dispersion of Pt on $MoO_x/MoSe_2$ electrodes, which were prepared by an intercalation–exfoliation technique. The $Pt/MoO_x/MoSe_2$ electrodes were tested for methanol oxidation by cyclic voltammetry. Thin films of $MoSe_2$ can be oxidized electrochemically to form a MoO_x layer. Compared with pure platinum, $Pt/MoO_x/MoSe_2$ electrodes gave lower oxidation potentials and higher current densities. We believe that methanol adsorption and subsequent dehydrogenation occur at the Pt atoms, while the OH_{ads} nucleation occurs at Mo sites. The presence of the adsorbed —OH groups on Mo sites may catalyze CO oxidation to CO_2. This surface reaction is necessary for the improved electrocatalytic behavior of $Pt/MoO_x/MoSe_2$ electrodes.

1. Introduction

The electrochemical oxidation of methanol has been widely investigated, because this fuel can be used in the direct methanol fuel cell [1]. Methanol is known to be oxidized to carbon dioxide at a platinum electrode in acid solution via several intermediates such as Pt_3C—OH and Pt—CO [2–5]. Methanol is a liquid fuel available at low cost. It can be easily handled, stored, and transported [6–9].

Platinum has shown the highest activity for methanol oxidation. However, the catalytic activity of the Pt electrode decreases considerably with time under use in a direct methanol fuel cell. This deactivation is mainly produced by the strong adsorption of CO_{ads} on the Pt surface. It has been postulated that the reaction follows parallel pathways forming dehydrogenated organic fragments on the platinum surface [10].

Platinum alloy or bimetallic electrodes have been used to reduce the poisoning and, therefore, to enhance the catalytic activity [11]. Compared to pure platinum, the most active electrocatalysts known so far are alloys of platinum and ruthenium, which exhibit lower overpotentials and extended lifetimes [12–14]. Molybdenum is also of particular interest for use with Pt because it reduces the overpotential for methanol or CO oxidation [15–18]. The characteristics of the $Pt_{75}Mo_{25}$ surface for the oxidation of H_2/CO mixtures have been found to be remarkably similar to those of $Pt_{50}Ru_{50}$ alloy [19]. This result was unexpected from the point of view of the difference in Ru and Mo chemistry [20]. It is believed that this second metal chemisorbs hydroxides or oxides necessary for the catalytic formation of CO_2 from CO [21, 22].

Since Mo is a promising metal that can be alloyed or mixed with platinum for the preparation of anode catalysts, we decided to develop a methodology by which this could be achieved using layered materials such as $MoSe_2$, in particular, with the demonstrated electrochemical stability of intercalated–exfoliated $MoSe_2$ thin films [23]. Layered materials such as MoS_2 and WS_2 have been combined with platinum black and tested for methanol oxidation [24]. Mo-based layered materials have shown promising electrochemical behavior.

Noble metals such as Pt, dispersed on high surface area inorganic oxides, are of considerable interest as high surface area catalysts [25]. The advantage of using a support such as $MoSe_2$ is that it can be electrochemically oxidized to produce an oxide layer on the film. This oxide surface will serve as a source of —OH groups necessary for the removal of adsorbed CO on Pt.

An intercalation–exfoliation method was used for the preparation of $MoSe_2$ thin films that served as supports for Pt and MoO_x. The final product was a $Pt/MoO_x/MoSe_2$ electrode. The deposition of the $MoSe_2$ flakes was on a Ti substrate. After the electrode was prepared, the MoO_x formation and deposition of Pt was done by cyclic voltammetry. The potential window used for this activation and deposition process was between 1.1 and −0.25 V vs SCE in 0.50 M H_2SO_4. For Pt electrodeposition, 1 mM potassium hexachloroplatinate in 0.50 M

H_2SO_4 was used. The product was a $MoO_x/MoSe_2$ surface covered with highly dispersed Pt microparticles. These electrodes were tested for methanol oxidation and compared to Pt electrodes.

2. Experimental

All chemicals, supplied by Acros Organics and Aldrich, were used as received. The preparation of the $MoSe_2$ thin films was carried out according to recently published research [23, 26, 27]. Briefly, 1.67 g of $MoSe_2$ was placed in a 150-ml volumetric flask, and in another flask 13 ml of 1.6 M *n*-butyl lithium in hexane solution was introduced under an inert atmosphere [28]. All the materials were introduced into an argon-filled dry box. The flask containing $MoSe_2$ was placed on a magnetic stirrer, and the 100 ml of hexane were added together with 13 ml of butyl lithium solution. The resulting solution was stirred for 48 h inside the dry box. After 48 h, it was filtered, and 24 h later the filtrate was weighed and placed in vials. For the exfoliation reaction, Li-intercalated $MoSe_2$ was placed in nanopure water. The beaker with the reactant and water was placed under ultrasound for 1 h [23, 28]. The final solid was added to 50 ml of nanopure water and 50 ml of hexane. The pH was lowered to 2.5 with 0.25 M HNO_3. The contents of the beaker with the fine layer of $MoSe_2$ were placed in a filter that contained several Ti platelets (0.5 cm^2). The exfoliated material was deposited on the Ti platelets while the rest of the solution passed through the filter. After 24 h, the surface-modified Ti platelets were dried under vacuum at 100 °C for 2 h. Each of the Ti platelets, covered with $MoSe_2$, were attached to a copper wire with silver paint and placed into a glass tube. Epoxy was used to cover the edges and ohmic contact area.

Each small $MoSe_2$-covered plaque was analyzed using a scanning electron microscope (SEM, JEOL JSM 5800 LV), with X-ray fluorescence detection. X-ray photoelectron spectroscopic (XPS) measurements were done with a PHI 5600ci multitechnique system.

The electrochemical measurements were made using a AFCBP1 Bipotentiostat (Pine Instrument, Grove City, Pennsylvania). The reference and counter electrodes were a saturated calomel electrode (SCE) and a platinum wire, respectively. Oxygen was removed from the solution by purging for 10 min prior to an experiment. The potential range used in all experiments was between +1.1 and −0.25 V vs SCE. For the electroactivation step, the electrode was cycled for 0.5, 1, 2 and 4 h in 0.50 M H_2SO_4 solution. For the electrodeposition of platinum, a solution 1 mM in potassium hexachloroplatinate (IV) (98%) and 0.50 M in H_2SO_4 was used. The electrodeposition of Pt was done by sweeping the potential between 1.1 and −0.25 V vs SCE, at various time increments. All solutions were prepared with water distilled and treated with a Nanopure System (Barnstead).

3. Results and discussion

Thin films of $MoSe_2$ can be electrooxidized electrochemically to form a MoO_x layer. We implemented this by cycling the potential at the $MoSe_2$ electrode in 0.50 M H_2SO_4 solution for 0.5, 1, 2, and 4 h. The objective was to find the optimal oxidation state, which assured optimal Pt deposition over the $MoO_x/MoSe_2$ layers. Figure 1 shows voltammograms for an $MoSe_2$ electrode for several electroactivation times. An increase in the capacitive current vs the activation time occurs, as expected for the greater roughness of the surface.

The elemental composition of the electrodes was monitored using X-ray fluorescence spectra (XRF). Figure 2 shows the spectra for $MoSe_2$ electrodes that had variable activation times plus 0.5 h of Pt electrodeposition. The XRF for Se, Mo, C, O, and Pt are presented in Figure 2(a). The XRF peaks of Mo and Se were expected, based on the original composition of the $MoSe_2$ material. The C peak represents atmospheric contamination. The O signal indicates the presence of oxides or hydroxides, products of the electroactivation of the surface. The Pt XRF peak confirms that Pt was electrodeposited on the electrodes.

The elemental composition of the electrodes determined by XRF is presented in Figure 2(b), which shows the composition for the electrodes that were electroactivated for 1 h. In this case, there are six elements present: C, O, Se, Mo, Pt, and Ti. However, the absence of the Ti signal in Figure 2(a), as compared to Figure 2(b), shows that some electrode material was lost, corresponding to a decrease in the layer thickness. The reason for this is that XRF photons arrive at the detector from the Ti plates that were used as substrates. The spectrum in Figure 2(c), a sample that was electroactivated for 2 h, shows six elements, as in Figure 2(b),

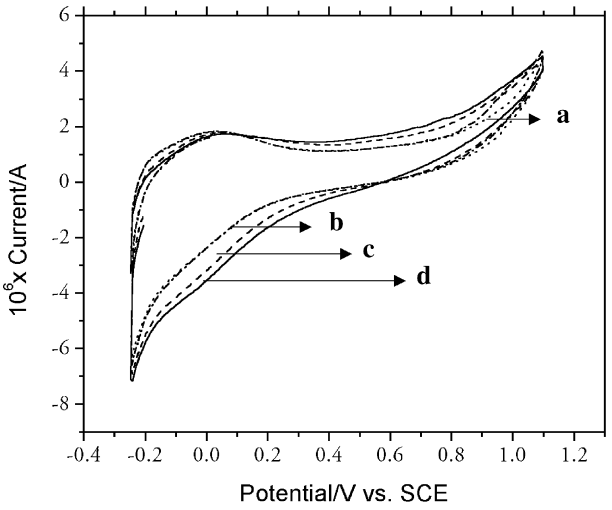

Fig. 1. Cyclic voltammograms of $MoSe_2$ electrodes in 0.50 M H_2SO_4 vs SCE. These electrodes were previously surface activated by cycling the potential between −0.25 and 1.1 V vs SCE in 0.50 M H_2SO_4 for a time of: (a) 0.5 h, (b) 1 h, (c) 2 h and (d) 4 h. All potential sweep scan rates were 100 mV s^{-1}.

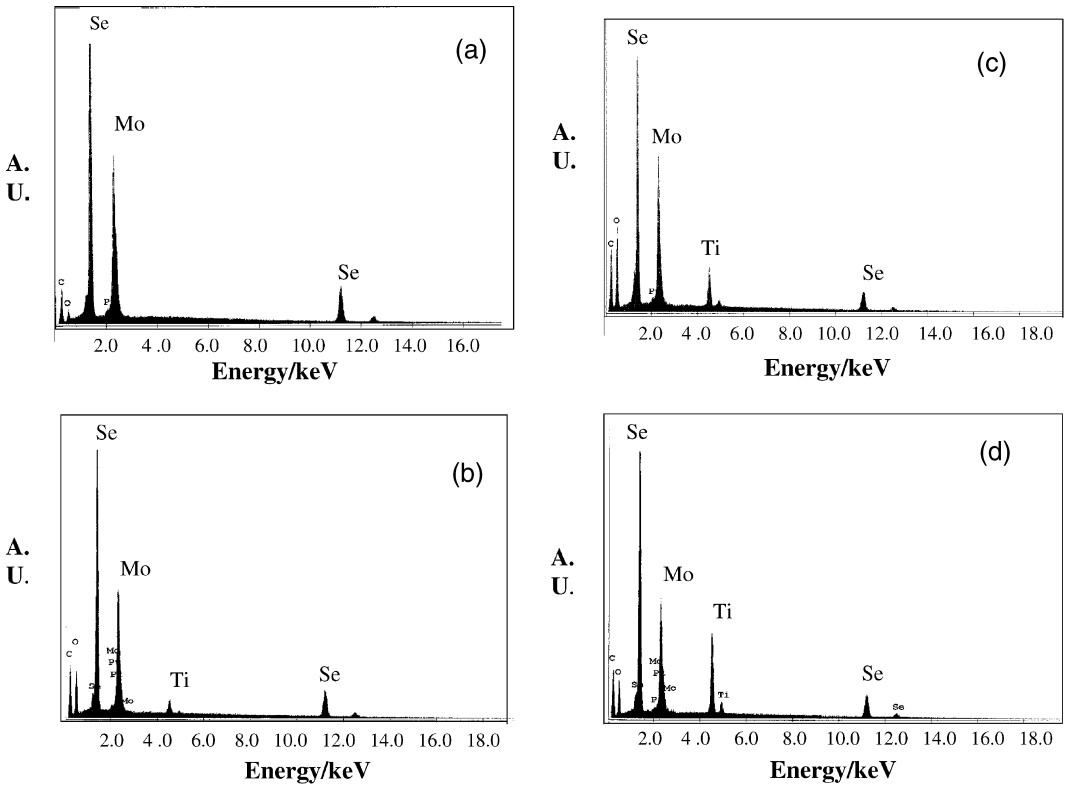

Fig. 2. X-ray fluorescence spectrum of a $MoSe_2$ electrodes with an excitation energy of 20 kV. The electrodes were electrochemically activated followed by Pt electrodeposition done by cycling between −0.25 and 1.1 V vs. SCE for 0.5 h in a solution of 1 mM K_2PtCl_6 and 0.50 M H_2SO_4. The electroactivation conditions and times were the same as in Figure 1: (a) 0.5 h, (b) 1 h, (c) 2 h and (d) 4 h. All potential sweep scan rates were 100 mV s^{-1}.

but in this case, the increase in the XRF intensity for Ti is noteworthy. Once again, this shows that the material is lost when the activation time is increased. The largest Ti XRF peak is present in Figure 2(d), for an electrode electroactivated for 4 h. This increasing loss of the $MoSe_2$ layers can be explained by higher oxidation states of molybdenum. The solubility increases when the oxidation state of Mo is higher than +4.

The electrodes, with the $MoSe_2$ thin films, were analyzed by scanning electron microscopy (SEM). This technique was used to study the morphology of the surface. Figure 3(a) shows a high roughness; this is important, because there is an increase in the surface area available for the electrodeposition of Pt. Figure 3(b) shows the morphology of the surface after 4 h of electroactivation time. In this case, the smaller surface area (i.e., lower roughness) is noteworthy. This finding agrees with the XRF data presented in Figures 2(a)–(d).

The elemental composition obtained by XRF was confirmed from the XPS analyses presented in Figure 4 for the $MoSe_2$ electrode. Figure 4(b) shows a high energy-resolution spectrum for the oxygen (1s) binding energy (BE) region. This energy region was evaluated with the objective of determining the various oxygen species present over the $MoSe_2$ layers and the consequent chemical changes obtained for these species when the electrodes are electroactivated. The XPS peak at a BE of 533.5 eV shows the presence of water. This peak is present when the electrode is analyzed prior to any electroactivation process. The XPS peak at 532.2 eV corresponds to a hydroxide species present over the surface of the $MoSe_2$ layer after an electroactivation of 2 h in 0.50 M H_2SO_4 solution. This process can be represented by the following equation:

$$MoSe_2 + H_2O \rightarrow MoSe_2{-}OH_{ads} + H^+ + e^- \qquad (1)$$

This electrooxidation process has been reported previously on well-ordered $MoSe_2$ surfaces [29, 30]. In agreement with the bifunctional mechanism, it is precisely these hydroxyl species that may inhibit the poisoning induced by CO, an intermediate in the methanol oxidation process [5].

The high energy resolution XPS spectrum for the molybdenum (3d) region is presented in Figure 4(c) for a $MoSe_2$ electrode. Each spectrum exhibits a $3d_{5/2}$–$3d_{3/2}$ doublet, due to spin–orbit coupling, which is separated in energy by 3.2 eV. Spectrum (1) corresponds to the $MoSe_2$ electrode before electrooxidation. The peak at 228.8 eV is due to Mo^{4+}. This oxidation state is characteristic of Mo in $MoSe_2$ compounds. Spectrum (2) in Figure 4(c) shows the XPS peak obtained after electroactivation of the $MoSe_2$ electrode for 2 h. Note the displacement to a more positive BE value. This can be attributed to an increase in the molybdenum oxidation state. It is clear that the Mo^{4+} species continues to be dominant, as expected from the stability of the $MoSe_2$ compound. The increase in the Mo oxidation

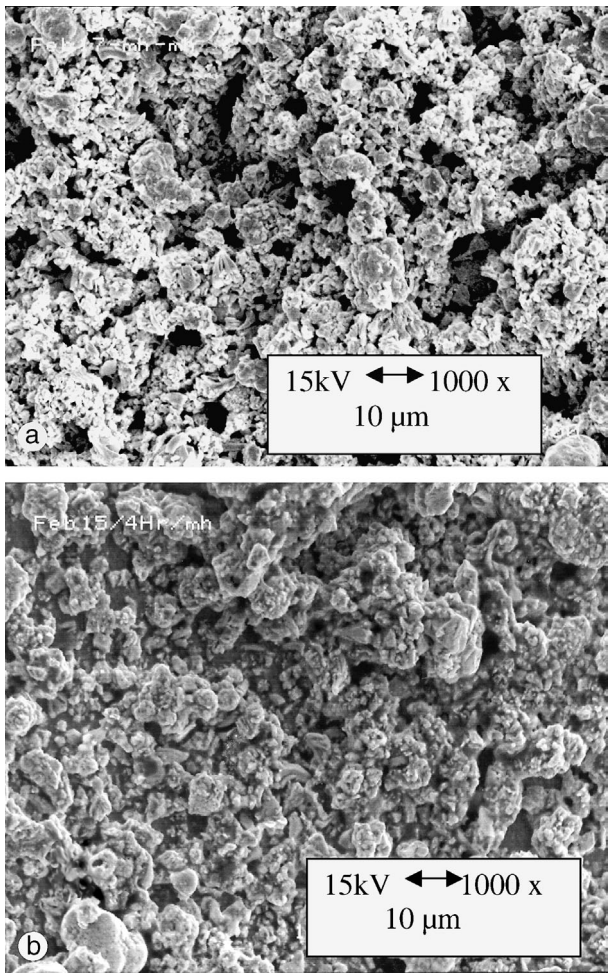

Fig. 3. SEM micrographs of $MoSe_2$ electrodes done at 15 keV and at a magnification of 1000×. These electrodes were electroactivated, followed by the electrodeposition of Pt for 0.5 h. The electroactivation conditions are the same as in Figure 1. The electroactivation time was of (a) 0.5 h and (b) 4 h. All potential sweep scan rates were 100 mV s^{-1}.

state, seen in spectrum (2) of Figure 4, is associated with an increase in the number of hydroxyls. This is in agreement with the oxygen species seen in the XPS spectrum corresponding to the O(1s) BE region (see Figure 4(b)).

Spectrum (3), in Figure 4c, corresponds to an electrode electroactivated for 4 h. By comparison with the corresponding O(1s) XPS BE region seen in Figure 4(a), it is clear that the hydroxyl species continues to be dominant, even though the XRF analysis indicates a loss of $MoSe_2$ film material. The Mo 3d BE region spectrum of an $MoO_x/MoSe_2$ electrode was deconvoluted in order to determine the various Mo species present. The deconvolution is shown in Figure 5 for an electrode electroactivated for 4 h. The Se (3s) XPS peak contribution is included in this spectrum, because it overlaps with the Mo (3d) XPS BE region. This was done by comparing the peak area obtained for Se (3d), whose BE peak appears at 56 eV, with the expected area for the Se (3s) peak. In order to make this comparison, we consider the sensitivity factor for each signal. In Figure 5, we can see a displacement of the BE peaks for the $3d_{5/2}$–$3d_{3/2}$ Mo doublet. In addition, we observe various oxidation states of Mo in the XPS curve-fitting. Fitting of the broader peaks reveals the existence of an Mo^{6+} species, as well as lower valence states such as Mo^{5+} and Mo^{4+}. When the oxidation state of Mo is increased, its solubility is also increased as well [29]. However, this may cause a loss of active sites.

Several mechanisms have been proposed for the methanol oxidation reaction. The most widely accepted is an initial adsorption of methanol on the platinum surface, with subsequent dehydrogenation. CO is an intermediate in the reaction, as seen in reaction 2 [22]. In order to convert CO directly to CO_2 the surface should have adsorbed OH species [12, 20]. The net result of the oxidation of methanol at Pt surfaces is the rapid surface coverage by a strongly bonded CO species, and, as a result, auto-inhibition of the catalytic process occurs. In the case of the $Pt/MoO_x/MoSe_2$ electrodes, the density of hydroxyl species is high, leading to the possible formation of CO_2 from CO.

The voltammetric curves for the $Pt/MoO_x/MoSe_2$ electrodes in 0.50 M H_2SO_4 after 1 h of Pt electrodeposition are shown in Figure 6. The electroactivation times were 0.5, 1, 2, and 4 h. A quantitative analysis of the areas under the hydrogen adsorption peaks shows the highest Pt surface areas for the electrodes that were electroactivated for 2 and 4 h. Although the amounts of Pt deposited on the electrodes electroactivated for 2 and 4 h were similar, their voltammetric curves show important differences. In the voltammetry of the electrode activated for 4 h, the peaks associated with Pt oxidation (starting at 0.7 V vs SCE) can be seen clearly. When the potential scan was reversed towards negative potentials, the cyclic voltammogram presented a peak associated with the reduction of the Pt oxide (starting at 0.7 vs SCE). On the other hand, in the electrodes electroactivated for 2 h, these Pt-associated peaks were considerably smaller.

The voltammetry for the electrode activated for 4 h is similar to that obtained for pure Pt, possibly because the Pt particles were deposited in too large a quantity, so that they formed agglomerates. It is clear that the 4-h electroactivation produces a considerable loss of material in the thin film, which represents a smaller area available for deposition of Pt particles. Although the amount of Pt in the electrode electroactivated for 2 h was greater than that in electroactivated for 4 h, the voltammetry obtained in the first scan shows that the Pt oxidation–reduction peaks were smaller in area. In this case, it is possible that there is poorer Pt dispersion on the $MoSe_2$ layer.

The $Pt/MoO_x/MoSe_2$ electrodes were tested for methanol oxidation using cyclic voltammetry. The solution was 0.50 M in H_2SO_4 and 0.50 M in CH_3OH. Figure 7 shows the results for $MoO_x/MoSe_2$ electrodes with electroactivation times of 0.5, 1, 2, and 4 h, plus 1 h of Pt electrodeposition. The electrode activated for 2 h gave the largest current and had a current onset

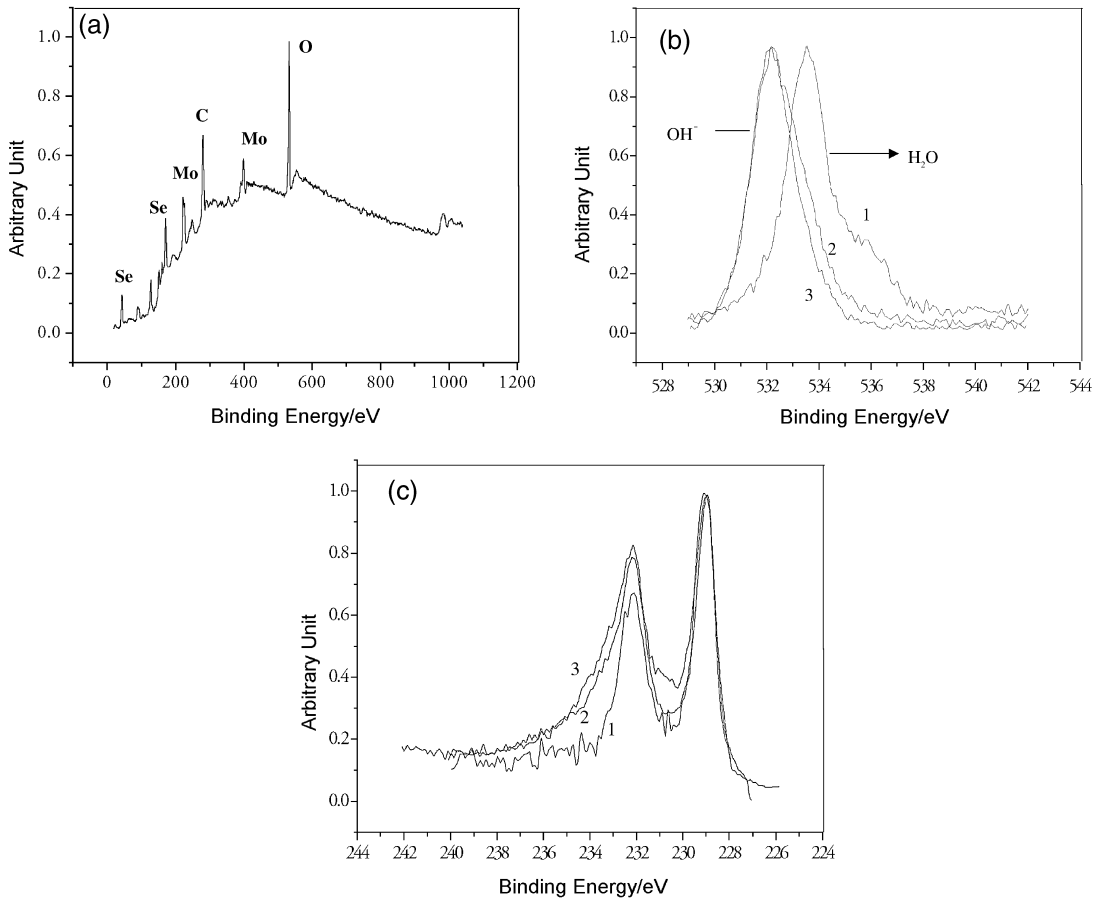

Fig. 4. (a) XPS survey spectrum of $MoSe_2$ electrodes using monocrhomatic radiation of Al$K\alpha$ as the excitation source. (b) High resolution XPS spectrum of the oxygen 1 s binding energy region: (1) before, (2) after 2 h and (3) after 4 h of electroactivation process in 0.50 M H_2SO_4. (c) High resolution XPS spectrum for the molybdenum 3d binding energy region: (1) before, (2) after 2 and (3) after 4 h of electroactivation process in 0.50 M H_2SO_4. The potential sweep scan rate, used in all the electroactivations, was 100 mV s^{-1}.

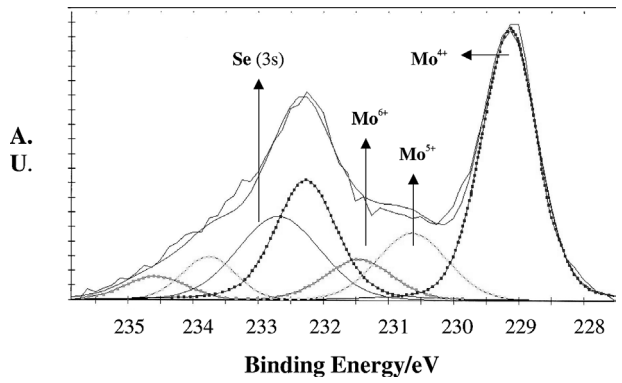

Fig. 5. Curve fitting of the high energy resolution XPS spectrum for the molybdenum 3d binding energy region for a $MoSe_2$ electrode which was electroactivated for 4 h using the conditions presented in Figure 1.

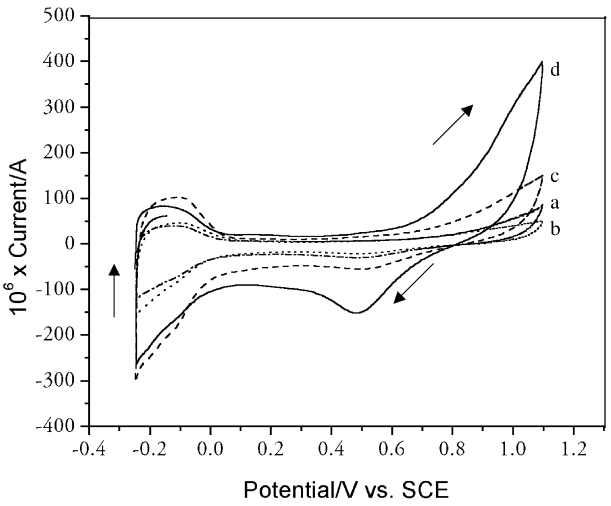

Fig. 6. Cyclic voltammograms of $Pt/MoO_x/MoSe_2$ electrodes in 0.50 M H_2SO_4. The electrodeposition of Pt was done by cycling the potential for 1 h between −0.25 and 1.1 V vs. SCE in 1 mM K_2PtCl_6 and 0.50 M H_2SO_4. The electroactivation time was of: (a) 0.5 h, (b) 1 h, (c) 2 h and (d) 4 h. The electroactivation conditions were the same as Figure 1. All potential sweep scan rates were 100 mV s^{-1}.

potential for methanol oxidation more negative than that for the other three electrodes. In Figure 6 the hydrogen adsorption–desorption areas are similar for electrodes electroactivated for 2 and 4 h. This indicates that the Pt surface area is similar for both electrodes. However, the voltammetric feature corresponding to the Pt oxidation–reduction region was smaller in area for the electrodes electroactivated for 2 h in 0.50 M H_2SO_4. This is an indication that a good interaction between the

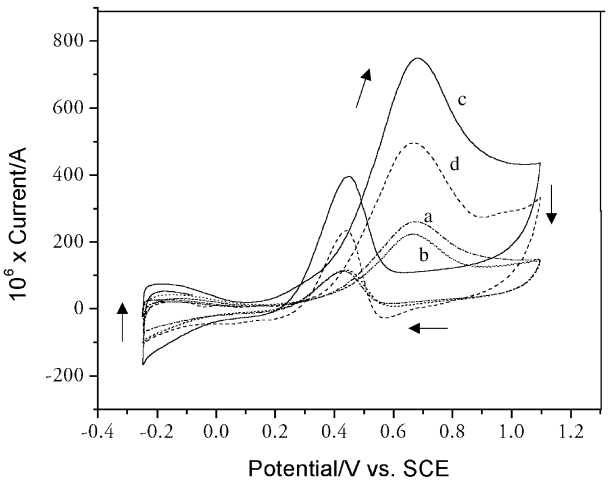

Fig. 7. Voltammogram of $Pt/MoO_x/MoSe_2$ electrode in 0.50 M H_2SO_4 and 0.50 M CH_3OH. The electrodeposition of Pt was done by cycling the potential for 1 h between −0.25 and 1.1 V vs SCE in 1 mM K_2PtCl_6 and 0.50 M H_2SO_4. The electroactivation conditions are the same as Figure 1. The activation time were: (a) 0.5 h, (b) 1 h, (c) 2 h and (d) 4 h. All potential sweep scan rates were 100 mV s^{-1}.

noble metal and the support is occurring. Therefore, an enhanced dispersion of the Pt submicroparticles into the molybdenum oxide films is expected. This can be translated to a better behavior of these electrodes for methanol oxidation. XPS analysis of the electrodes electroactivated for 2 h showed the highest hydroxide species concentration on the $MoSe_2$ thin film (see Figure 4), therefore facilitating the promotion of the oxidation of undesirable intermediates like CO to CO_2.

One way to observe the possible increase in the oxidative capacity of $Pt/MoO_x/MoSe_2$ electrodes is by comparing their voltammetry with that of a reference. In our case, we used a pure Pt electrode as reference in the methanol oxidation. Figure 8 shows the voltammetry of the Pt and $Pt/MoO_x/MoSe_2$ electrodes. Both currents were normalized by the Pt surface area. This was done by using the integration of charge associated with hydrogen adsorption on the Pt surface in 0.50 M H_2SO_4. The cyclic voltammetry of the $MoSe_2$ electrode (Figure 1) showed an increase in current with electroactivation time in the potential region 0.2 to −0.2 V vs SCE. These currents overlap the hydrogen adsorption–desorption region for the $Pt/MoO_x/MoSe_2$ electrode (Figure 6). However, the current scale in Figure 6 is 100 times larger than that in Figure 1. This makes the $MoSe_2$ double layer contribution negligible in the estimation of the Pt surface area for $Pt/MoO_x/MoSe_2$.

In all the calculations, we used the normally accepted value of 210 $\mu C\ cm^{-2}$ for hydrogen adsorption on polycrystalline Pt. Based on our results, the $Pt/MoO_x/$

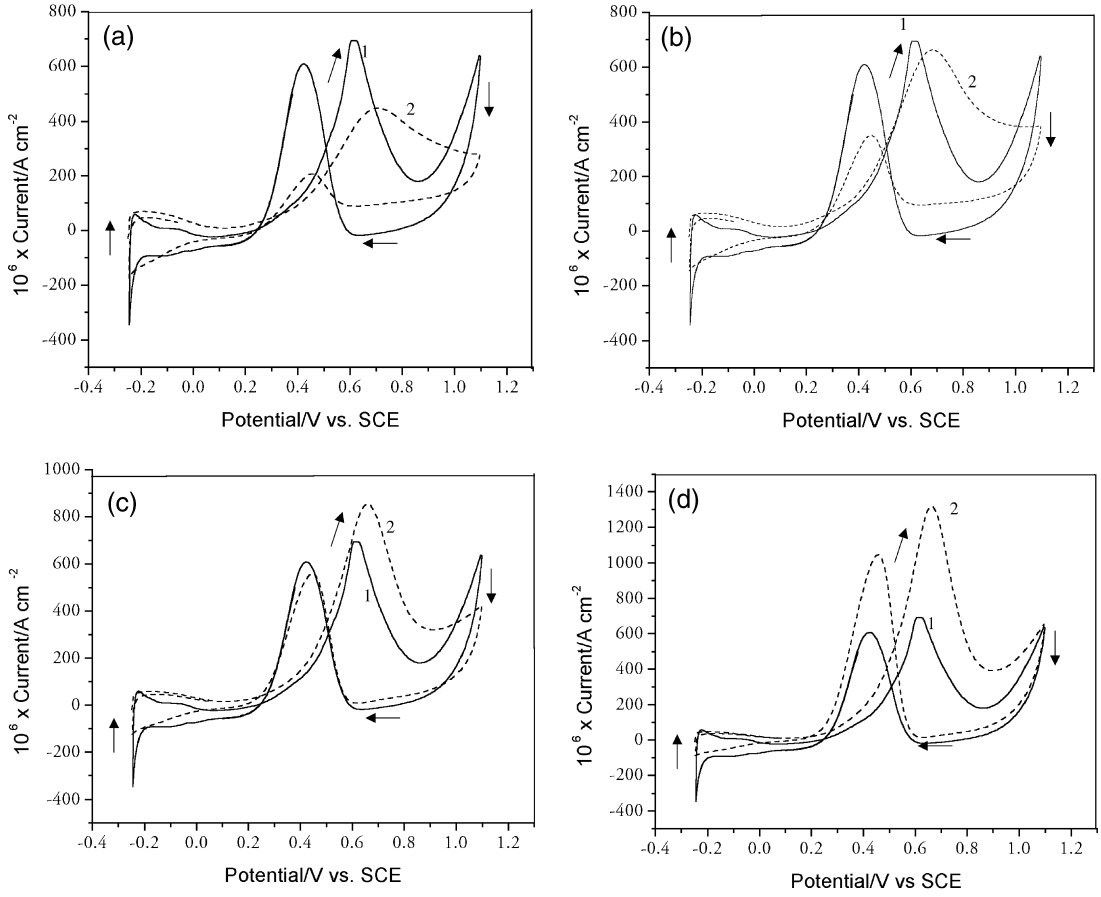

Fig. 8. Cyclic voltammograms with the current normalized by real Pt surface area for (1) Pt electrode and (2) $Pt/MoO_x/MoSe_2$ electrodes in 0.50 M H_2SO_4 and 0.50 M CH_3OH. The electrodeposition time of Pt were (a) 0.5 h (b) 1 h (c) 2 h and (d) 4 h. These electrodes were previously surface activated by cycling the potential between −0.25 and 1.1 V vs SCE in 0.50 M H_2SO_4 for 2 h.

$MoSe_2$ electrode was electroactivated for 2 h with the objective of assuring the optimal hydroxide concentration on the surface.

The Pt deposition time of the $Pt/MoO_x/MoSe_2$ electrode in Figure 8(a) was 0.5 h. The current density obtained for the Pt electrode was higher than that for the $Pt/MoO_x/MoSe_2$ electrode in the methanol oxidation process. This behavior can possibly be explained by the Pt dispersion being too large in $Pt/MoO_x/MoSe_2$. This excessive dispersion blocks the optimal methanol adsorption necessary to start the oxidation. Nevertheless, the methanol oxidation current does not decay as quickly compared with the pure Pt electrode. In the $Pt/MoO_x/MoSe_2$ electrode, a larger current persists after the first oxidation peak, until the potential is reversed towards negative values. This may indicate that it is not necessary to wait for hydroxide formation on the Pt surface to promote CO to CO_2. This promotion may occur according to the following mechanism:

$$Pt{-}CO_{ads} + MoSe_2{-}OH_{ads} \rightarrow Pt + MoSe_2 + CO_2 + e^- + H^+ \quad (2)$$

In the case of Pt, an alternate mechanism may be followed:

$$Pt{-}CO_{ads} + Pt{-}OH_{ads} \rightarrow 2Pt + CO_2 + H^+ + e^- \quad (3)$$

From the XPS spectra, almost all the oxygenated species present on the $Pt/MoO_x/MoSe_2$ surface are —OH. The methanol oxidation reaction is more feasible when the concentration of hydroxyl species on the surface is larger.

Figure 8(b) shows the voltammetry for the $Pt/MoO_x/MoSe_2$ electrode for which the Pt electrodeposition was 1 h. A slight improvement in current density is seen when compared to the pure Pt electrode. In Figures 8(c) and (d), the $Pt/MoO_x/MoSe_2$ electrodes had Pt deposition times of 2 and 4 h, respectively. In both figures, the current densities were higher than that for the Pt electrode. The current onset potentials were more negative than that for pure Pt. For these cases, the Pt dispersion may be smaller because of the greater amount of Pt deposited. This low dispersion seems to favor better adsorption of the methanol molecule. In summary, the best $Pt/MoO_x/MoSe_2$ electrode for methanol oxidation was that electroactivated for 2 h in 0.50 M H_2SO_4 and then subjected to 4 h of Pt electrodeposition.

4. Conclusions

$Pt/MoO_x/MoSe_2$ electrodes were prepared with Li intercalation and exfoliated $MoSe_2$. This material was used as a support for the electrodeposition of platinum to take advantage of its high surface area, its stability in acid solution and the enhanced catalytic activity of platinum in the presence of Mo oxide species. By use of cyclic voltammetry, it was possible to control the degree of Mo oxidation in the $MoSe_2$ thin layer. This change in the molybdenum oxidation state is associated with an increase in the concentration of oxide species. It is clear that the adsorption of oxygen-containing species on the $Pt/MoO_x/MoSe_2$ electrodes commences at lower potentials compared with the platinum electrode. It is believed that the oxygen-containing surface species is responsible for the lower current onset potential for the oxidation of methanol compared to pure Pt electrodes. The $Pt/MoO_x/MoSe_2$ electrodes have shown good electrocatalytic properties for methanol oxidation. In addition, their high stability under continuous use for methanol oxidation presents an alternative for application in fuel cell technology.

Acknowledgements

This work was supported by DOD-EPSCoR Grant DAAH04-96-1-0199 and the ARL Collaborative Technology Alliance in Power and Energy, Cooperative Agreement no. DAAD19-01-2-0010. The surface analysis facility was provided by the Materials Characterization Center of the University of Puerto Rico at Río Piedras. Mr Gabriel Cruz and Ms Emerilis Casado are acknowledged for their technical assistance.

References

1. N.H. Li, S.G. Sun and S.P. Chen, *J. Electroanal. Chem.* **430** (1997) 57.
2. A. Kelaidopoulou, E. Abelidou and G.J. Kokkinidis, *J. Appl. Electrochem.* **29** (1999) 1255.
3. S.G. Sun, L.G. Quiang and T.Z. Wu, *J. Electroanal. Chem.* **393** (1995) 97.
4. V.S. Bagotzky, Y.B. Vassilev and O.A. Khazova, *J. Electroanal. Chem.* **81** (1997) 229.
5. H. Hu and I.E. Wachs, *J. Phys. Chem.* **99** (1995) 10911.
6. J. Wang, S. Wasmus and R.F. Savinell, *J. Electrochem. Soc.* **142** (1995) 4218.
7. J.G. Love, P.A. Brooksby and A.J. McQuilan, *J. Electroanal. Chem.* **464** (1999) 93.
8. H.N. Dinh, X. Ren, F.H. Garzon, P. Zelenay and S. Gottesfeld, *J. Electroanal. Chem.* **491** (2000) 222.
9. M. Gotz and H. Wendt, *Electrochim. Acta* **43** (1998) 3637.
10. B.D. McNicol, *J. Electroanal. Chem.* **118** 71 (1981).
11. K. Lasch, G. Hayn, L. Jorissen, J. Garche and O. Besenhardt, *J. Power Sources* **105** (2002) 203.
12. H.A. Gasteiger, N. Markovich, P. Ross and E.J. Cairns, *J. Phys. Chem.* **97** (1993) 12020.
13. H. Kim, I.R. Moraes, G.T. Filho, R. Haasch and A. Wieckowski, *Surf. Sci.* **474** (2001) L203.
14. Y. Ishikawa, M.S. Liao and C.R. Cabrera, *Surf. Sci.* **66** (2000) 463.
15. H. Nakajima and H. Kita, *Electrochim. Acta* **35** (1990) 849.
16. P. Gourérec, M.C. Denis, D. Guay, J.P. Dodelet and R. Schulz, *J. Electrochem. Soc.* **147** (2000) 3989.
17. N. Narishige and M. Niwa, *Catal. Lett.* **71** (2001) 63.
18. Z. Jusys, T.J. Schmidt, L. Dubau, K. Lasch, L. Jorissen, J. Garche and R.J. Behm, *J. Power Sources* **105** (2002) 195.
19. B.N. Grgur, G. Zhuang, N.M. Markovich and P.N. Ross, *J. Phys. Chem.* **101** (1997) 3910.
20. B.N. Grgur, N.M. Markovich and P.N. Ross, *J. Phys. Chem.* **102** (1998) 2494.

21. D.R. Rolison, P.L. Hagans, K.E. Swider and J.W. Long, *Langmuir* **15** (1999) 774.
22. A. Couto, M.C. Pérez, A. Rincón and C. Gutiérrez, *J. Phys. Chem.* **100** (1996) 19538.
23. R.J. Castro and C.R. Cabrera, *J. Electrochem. Soc.* **9** (1997) 3135.
24. H. Binder, A. Kohling and G. Sandstede, *in* G. Sandstede (Ed.), 'From Electrocatalysis to Fuel Cells', (University of Washington Press, 1972), pp. 59–79.
25. H. Hixson and P. Sherwood, *Chem. Mater.* **8** (1996) 2643.
26. Y. Santiago and C.R. Cabrera, *J. Electrochem. Soc.* **141** (1994) 629.
27. P. Joensen, R.F. Frindt and S.R. Morrison, *R. Mat. Res. Bull.* **21** (1986) 457.
28. M.B. Dines, *Mat. Res. Bull.* **10** (1997) 287.
29. R.J. Castro and C.R. Cabrera, *Langmuir* **11** (1995) 1375.
30. T. Ohmori, R.J. Castro and C.R. Cabrera, *Langmuir* **14** (1998) 6755.